Lunar Laser Ranging Instrument (LLRI): a tool for the study of topography and gravitational field of the Moon

J. A. Kamalakar*, A. S. Laxmi Prasad, K. V. S. Bhaskar, P. Selvaraj, R. Venkateswaran, K. Kalyani, A. Goswami and V. L. N. Sridhar Raja

Laboratory for Electro-Optics Systems, Indian Space Research Organization, Bangalore 560 058, India

The Lunar Laser Ranging Instrument (LLRI) developed for flight on the Chandrayaan-1 spacecraft was designed to measure the topography of the lunar surface over a 2-year period from a 100 km polar orbit of Moon. A 10 mJ diode-pumped pulsed laser together with 200 mm diameter telescope and a silicon avalanche photodiode are the principal optical assemblies of this active remote-sensing instrument. We present here science objectives of LLRI and its performance specifications along with details of instrument design. The methods by means of which LLRI performance and operability were analysed are also presented. During end-to-end testing, the integrated LLRI was operated in free space aiming at a distant target (~30 km). Test results were found to be satisfactory and well within the desired specifications.

Keywords: Laser altimeter, Moon, topography.

Introduction

THE Moon with the history of the early solar system etched on it provides a pathway to unravel the early evolution of the solar system and that of the planet earth. The current decade saw a rejuvenated interest in exploration of the Moon. In late 2008, the first Indian spacecraft Chandrayaan-1 placed eleven scientific payloads in the polar orbit of the Moon with the objective of further our understanding of the Moon based on high resolution selenological studies, and chemical and mineral mapping of the lunar surface[1]. One of these instruments, the Lunar Laser Ranging Instrument[2] (LLRI), will use infrared laser pulses to provide altimetry data that will accurately map topology of the Moon. In addition to gathering data typical of previously flown lunar altimeters[3–5], the LLRI will obtain altimetry data close to the lunar polar region. High-precision altimetry data will contribute significant insight into lunar evolution. In particular, LLRI data will provide an improved model of the lunar gravitational field for better understanding of the geophysics of the Moon. This instrument supplements another Indian payload namely the Terrain Mapping Camera (TMC). LLRI is designed to operate continuously throughout the planned mission life of two years and produce precision altimetry data over the entire lunar surface. The laser altimeter detects round-trip time, or time of flight (TOF), using a high-power pulsed laser with precise timing measurements, which provide range resolution of better than 25 cm. To validate the LLRI design and to ensure its successful operation on board Chandrayaan-1, several instrument-level and integration tests were devised and performed. These included an operational test sequence of LLRI to verify correct 'end-to-end' system operation and characterization of instrument performance. End-to-end testing also provided information associated with operational peculiarities of the LLRI and was vital for the checkout of the instrument–spacecraft interface. Figure 1 shows the flight version of LLRI on the deck of Chandrayaan-1 spacecraft during integration checks. The LLRI performance specifications are summarized in Table 1.

LLRI system design

The design and development choices were tightly constrained from the outset, principally by schedule and space-

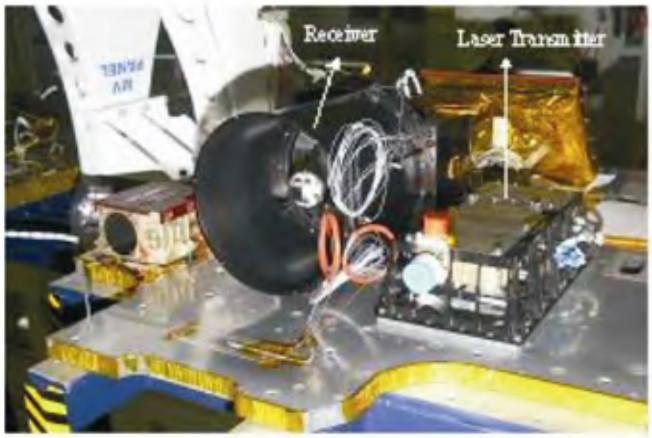

Figure 1. Flight version of LLRI on Chandrayaan-1's spacecraft deck.

*For correspondence. (e-mail: kamalakar@leos.gov.in)

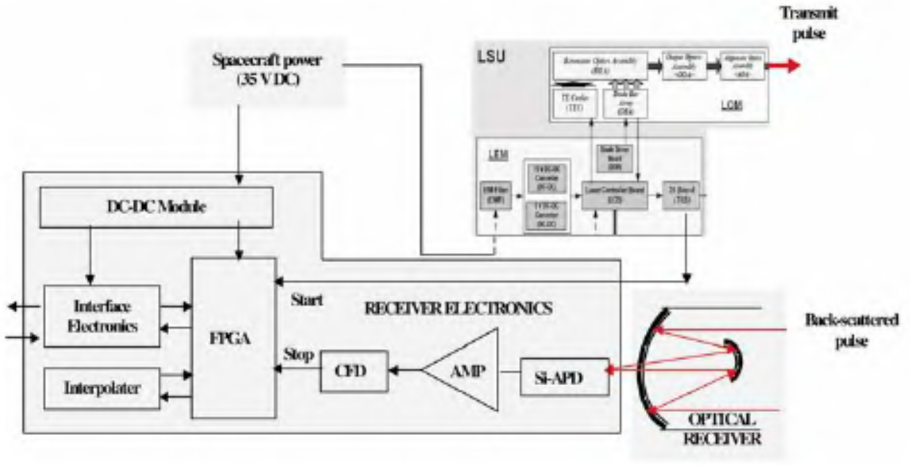

Figure 2. Block diagram of LLRI with its subsystems.

Table 1. Specifications of Lunar Laser Ranging Instrument

Parameter	Specification
Maximum range	100 km (>100 km)
Range accuracy	≤ 5 m (<5 m)
Range resolution	≤ 5 m (<1.5 m coarse, <25 cm fine)
Instrument weight	10 kg
Instrument power	25 W
Data update rate	10 Hz
Operational period	2 years continuous
Dimension	470 × 380 × 280 mm

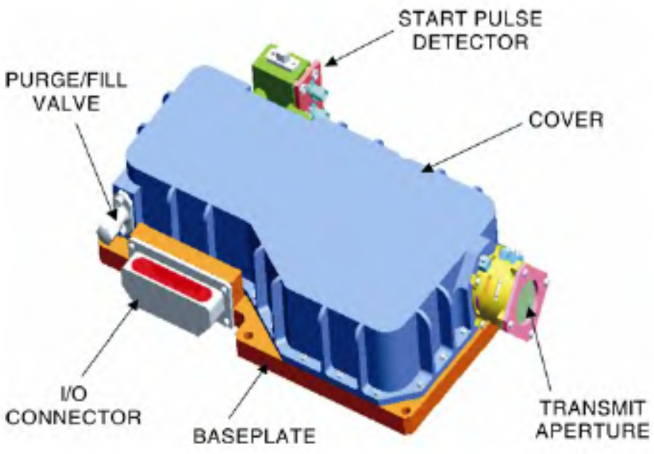

Figure 3. Nd : YAG laser optics module.

craft accommodation. Figure 2 shows the block diagram of the LLRI with its subsystems. The LLRI payload consists of an optical assembly, an electronics package, and a support structure. The optical assembly contains the laser transmitter and receiver subsystems. As per the mission requirements, a diode-pumped Q-switch Nd : YAG laser oscillator with maximum performance of 10 mJ pulse energy at 1064 nm wavelength was opted[6–9]. Following fabrication of the transmitter, receiver optics and electronics, integration and acceptance tests at the instrument level was taken up. The integrated LLRI was subsequently tested and flight qualified at both instrument and spacecraft levels. Figure 3 depicts a rough sketch of the laser module used. Receiver design uses a lightweight Cassegrain telescope, a spectral filter (centred at the laser wavelength) and a single-element avalanche photodiode (APD) hybrid detector. A significant aspect of our configuration is that the LLRI receiver optics acts as a direct-detection 'photon bucket'. This approach drastically simplified the design and development of the optical receiver because the system is not required to produce an image. Consequently, the optics could tolerate high levels of aberrations as long as the resultant spot size remained within the physical and alignment bounds of the APD detector. This allows us to select the receiver optical design best suited for low weight and manufacturing ease, specifically, a Dall–Kirkham design (Figure 4).

Our telescope is a 2-mirror zerodur Dall–Kirkham arrangement. The primary mirror diameter is 200 mm with overall receiver field of view of ± 0.025°. Table 2 displays the LLRI design parameters as per specifications as well as measured/confirmed observations. The overall mass of telescope structure was 1600 g. Acceptance testing indicated that 98% of the focused energy was located within a 130 μm central (Airy) disk, easily accommodated by the 800 μm active diameter of the APD detector.

Details of the LLRI instrument electronics are provided by Kamalakar *et al.*[2]. The main sub-elements of the receiver electronics are the detector, constant fraction discriminators (CFD) and time digitizer unit (TDU) as shown in Figure 2. The input signal to the receiver is a small fraction of the reflected laser pulse from the lunar surface collected by the receiver telescope. Considering the factors like size, sensitivity, speed of response and ease of use, Si APD is chosen for LLRI[10]. An added advantage of using Si APD is that the internal gain mechanism of APD improves the sensitivity of the diode as compared to PIN diodes.

In-line optical alignment

For any typical instrument intended for the applications like range measurement[11,12], alignment of transmitter and receiver fields of view plays a vital role to achieve the best reliable outcome. The payload transmitter and receiver bore-sight alignment involve a 3-step procedure: (i) cross-check of receiver focal point on the detector's active area, (ii) finding an optimized position for the detector, and (iii) bore-sight of the transmitter and receiver alignment. In the first step, receiver focal point on the detector's active area was checked by employing an interference technique. Depending on the co-linearity of the spot images (i.e. interference fringe pattern produced by Zygo interferometer) and through minute adjustments, optical receiver focal point was made close to detector's active area. Because of the small field of view of the LLRI receiver, placement of the detector is one of the prime concerns for achieving the optimum signal-to-noise performance. This was done by measuring the receiver field of view in both azimuth and elevation directions in front of off-axis collimator by monitoring the signal through APD[13]. In the final step, a pair of 45°-mirror assembly was used to align the bore-sight of the transmitter and receiver system taking receiver cube axis as reference (see Figure 5). Alignment accuracy (in arc seconds) was further improved by placing a CCD camera in front of receiver optics. By monitoring the laser spot image captured by CCD, transmitter was aligned in line to the receiver axis through micro-level movements of Risley prism (at exit aperture of laser transmitter) taking image centroid as reference. Finally, the alignment was confirmed by monitoring the signal at the detector.

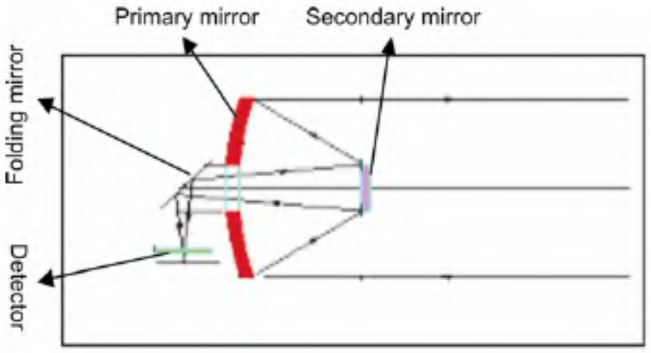

Figure 4. Dall–Krikham design for the LLRI receiver telescope.

Figure 5. Alignment scheme followed to bring the laser transmitter in line to receiver axis.

LLRI testing and performance analysis

LLRI testing include functional (namely initial bench test, transmitter and receiver alignment, initial field/range test), environmental (thermal vacuum cycling test, vibration test) and end-to-end testing both at the instrument and spacecraft levels.

Functional testing

Under this scheme different range simulating techniques[14], viz. FORS (fiber-optic range simulator, to simulate range up to 20 km) and GCRS for long ranges (ground check range simulator) were employed. GCRS generates user-defined time-delays to simulate the range up to 1000 km. This simulator detects the start laser signal from LLRI transmitter and provides an optical stop pulse to LLRI receiver after a user defined timing delay. In our experiments, we have defined seven time delays covering the range from 2 to 200 km and instrument performance was checked by observing the time gap between start and stop pulses as detected by the LLRI receiver electronics. For a constant optical delay of 53 μs produced by GCRS, the measured delay after integration calibration range counter during testing allowed us to determine the quality of the instrument measurements based on threshold levels selected, operational modes selected and various environmental conditions. Figure 6 is a range plot collected by LLRI-console software for a fixed delay of 53.3 μs (equivalent to the 8 km range) by GCRS. This type of functional testing allowed us to detect range-walk caused by changes in threshold level.

Environmental testing

LLRI was subjected to rigorous environmental conditions. We have placed the entire integrated instrument in a thermal vacuum chamber and operated it over several thermal cycles at extreme temperatures (0°C to +40°C). To characterize the LLRI while it was in the chamber, we have introduced the GCRS that permitted continuous performance evaluation. To prevent corona and ensure reliable operation, the instrument was soaked in vacuum before it was powered. We plotted the range generated by LLRI using delay produced by GCRS and monitored all necessary instrument parameters at three temperature levels, 0°C, ambient and +40°C. Very little thermal influence on LLRI performance was found over the entire temperature range. The instrument was then subjected to mechanical

Table 2. LLRI design parameters

Parameter	Specification	Measurement/conformance
Transmitter wavelength	1064 nm	1064.40 ± 1 nm
Operating mode	Pulsed	Complies
Pulse energy (min)	10 mJ	11.9 mJ
Pulse energy stability	Energy jitter (peak) < ± 10%	Energy variation (peak) < ± 4%
Spectral bandwidth	0.05 nm	±0.05 nm
Pulse repetition rate	10 Hz	10 Hz
Pulse width	4–5 ns (FWHM)	<2 ns
Beam divergence (full)	<0.5 mrad	0.324 mrad
Lifetime (shots)	$>1 \times 10^6$	Complies
Spectral receiver bandwidth	<10 nm	Complies
Detector	Silicon APD	Complies
APD responsivity	200 kV/W@1064 nm	200 kV/W
Optical receiver FOV	0.05°	0.051°
Threshold levels	N/A	4
Tx/Rx alignment shift due to vibration	<36″ in each direction	23″ in azimuth* 27″ in elevation*

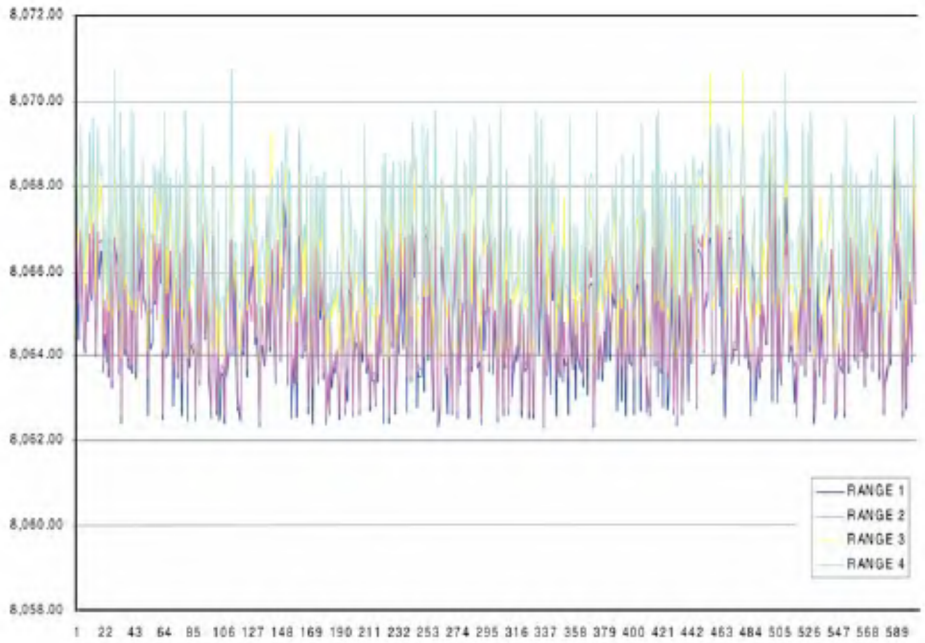

Figure 6. Range plot generated by LLRI for a simulated delay of 53.3 μs by GCRS (range-walk can also be seen in the plot).

vibration test, which involved frequency swept vibration levels, mechanically induced from 20 to 2000 Hz at slope rate of 3 dB/octave. LLRI payload was not ON during mechanical environment test and no functional test is performed. The pre- and post-vibration alignment for LLRI payload was carried out taking separate references for transmitter and receiver optical axes. For transmitter, the laser beam was focused onto a CCD and the spot was being monitored taking its centroid as reference. For receiver, a semiconductor pulsed laser diode through an off-axis autocollimator was focused onto receiver optics by aligning the laser diode beam to receiver optical reference axis. The APD pre-amplifier output was measured in elevation and azimuth from the reference axis and compared with pre- and post-vibration observations. The LLRI flight model vibration levels are finalized after performing low low-level sine search for each axis. The vibration levels in all the 3-axes have been notched at amplification points.

Field test

Finally, LLRI performance was checked during field tests by receiving back-scattered signal bouncing from the distant natural targets like buildings and distant hills on laser illumination from transmitter and range was computed

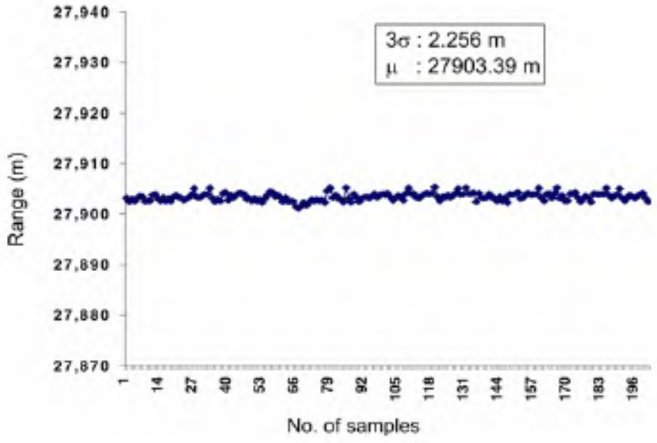

Figure 7. Range plot for a distance of 28 km during field test.

from each target by measuring round-trip travel time of signal both in pre- and post-environmental and functional tests. Measured range with a standard laser range finder up to few kilometers confirmed the accuracy of LLRI. Figure 7 shows the range plot during field test for 28 km range generated by LLRI on sending the pulses to a distant hill. The signal received from 28 km target when extrapolated to 100 km Moon's orbit after taking into atmospheric attenuation is around 5–7 times the threshold value.

Conclusion

Although the LLRI is like other terrestrial laser range finders, the combined requirement of operating an instrument in deep space for a long period of two years under strong design constraints contributed significantly to the complexity of the instrument. The performance of the instrument matched the desired specifications in all aspects and proved its reliability and efficiency. Data obtained by LLRI during Chandrayaan-1 mission will further our understanding of lunar global topography and gravity field.

1. Goswami, J. N., Thyagarajan, K. and Annadurai, M., Chandrayaan-1: Indian mission to moon. *Lunar Planet. Sci.*, 2006, **XXXVII**, 1704.
2. Kamalakar, J. A., Bhaskar, K. V. S., Laxmi Prasad, A. S., Ranjith, R., Lohar, K. A., Venketeswaran, R. and Alex, T. K., Lunar ranging instrument for Chandrayaan-1. *J. Earth Syst. Sci.*, 2005, **114**, 725–731.
3. Riris, H., Xiaoli, S., Cavanaugh, J. F., Jackson, G. B., Ramos-Izquierdo, L., Smith, David, E. and Zuber, M., The lunar orbiter laser altimeter (LOLA) on NASA's lunar reconnaissance orbiter (LRO) mission, sensors and systems for space applications. *Proc. SPIE*, 2007, **6555**, 65550I.
4. Araki, H., Ooe, M., Tsubukova, T., Kawano, N., Hanada, H. and Heki, K., Lunar laser altimetry in the SELENE project. *Adv. Space Res.*, 1999, **23**, 1813–1816.
5. Shu, R., Wang, J, Hu, Y. and Jia, J., The development of the CHANG'E-1 lunar explorer laser altimeter, Shanghai Institute of Technical Physics, 36th COSPAR Scientific Assembly, Chinese Academy of Sciences, Beijing, China, July 2006.
6. Coyle, D. B., Kay, R. B., Stysley, P. R. and Poulios, D., Efficient, reliable, long-lifetime, diode-pumped Nd : YAG laser for space-based vegetation topographical altimetry. *Appl. Opt.*, 2004, **43**, 5236–5242.
7. Krebs, D. J., Novo-Gradac, A.-M., Li, S. X., Lindauer, S. J., Afzal, R. S. and Yu, A. W., Compact, passively Q-switched Nd : YAG laser for the MESSENGER mission to Mercury. *Appl. Opt.*, 2005, **44**, 1715–1718.
8. Fan, T. Y. and Byer, R. L., Diode laser-pumped solid-state lasers. Quantum electronics. *IEEE J.*, 1988, **24**, 895–912.
9. Hughes D. W. *et al.*, Laser diode pumped solid state lasers. *J. Phys. D: Appl. Phys.*, 1992, **25**, 563–586.
10. Sridhar Raja, V. L. N., Ranjith, R., Bhaskar, K. V. S. and Laxmi Prasad, A. S., Avalanche photodiode (APD) for space applications. Proceedings of 12th National Seminar on Physics and Technology of Sensors, 2007, pp. 81–83.
11. Bender, P. L. *et al.*, The lunar laser ranging experiment. *Science*, 1973, **182**, 229.
12. Cole, T. D., NEAR laser rangefinder: A tool for the mapping and topologic study of Asteriod 433 Eros. *John Hopkins APL Techn. Digest*, 1998, **19**, 142–157.
13. Sridhar Raja, V. L. N., Selvaraj, P., Adwaita, G., Kalyani, K., Bhaskar, K. V. S., Laxmi, Prasad, A. S. and Kamalakar, J. A., Optical alignment procedure for position optimization of an IR detector used in Lunar Laser Range Instrument (LLRI). Proceedings of XXXIII OSI Symposium on Optics and Optoelectronics, Tezpur, 2007.
14. Goswami, A., Ranjith, R., Bhaskar, K. V. S., Laxmi Prasad, A. S. and Kamalakar, J. A., Fiber Optic Range Simulator (FORS) for Lunar Laser Ranging Instrument (LLRI). Proceedings of XXXIII OSI Symposium on Optics and Optoelectronics, Tezpur, 2007.

ACKNOWLEDGEMENTS. We thank Mr Y. K. Jain (Deputy Director) and Dr T. K. Alex (Director) for the inputs and suggestions provided during the system realization and development.